Relaxation oscillations of the synchrotron motion caused by narrow-band impedances

C. Limborg and J. Sebek
Stanford Synchrotron Radiation Laboratory/Stanford Linear Accelerator Center, MS 99, P.O. Box 4349, Stanford, California 94309
(Received 19 April 1999)

Although the linearized theory of small amplitude synchrotron oscillations and the instability thresholds derived from it have long been understood, there is no satisfactory description of the large amplitude highly nonlinear synchrotron motion of a bunched beam. With an appropriate tuning of the RF cavity impedance, large amplitude, low frequency, self-sustained relaxation oscillations of this synchrotron motion are generated. This paper presents detailed experimental data on such behavior, tracking code results that reproduce the important characteristics, and a simple analytical model that explains the key features of the relaxation oscillation: growth of the instability, saturation of the oscillation, breakup of the bunch, and subsequent damping of the system back to the beginning of the next cycle of the relaxation oscillation. [S1063-651X(99)10110-7]

PACS number(s): 29.27.Bd, 05.45.−a

I. INTRODUCTION

To describe the complicated motion of a charged particle beam in a storage ring, one uses equations that can be transformed, with the appropriate sets of variables, into those of a perturbed harmonic oscillator. In the transverse planes, this transformation leads to a Hill equation [1] and the restoring forces come from external magnetic fields. In the longitudinal plane, the exact single particle equation is that of a circular pendulum, with the RF electric field providing the restoring force. For sufficiently small amplitudes of motion, the systems can be well described by the harmonic oscillator equation. We refer to this as the linear regime. Electron machines also have natural damping as a consequence of significant synchrotron radiation emission. In addition, particles generate electromagnetic fields that act as a driving force, perturbing the focusing and stability of the beam. Depending on their characteristics, these perturbations can either provide stability to the beam or drive it to instability. The linear theory that explains the threshold of coupled bunch instabilities has long been understood. Large forced oscillations have been studied and described for both proton [2] and electron [3] machines. It has also long been observed that especially for synchrotron oscillations, i.e., those in the longitudinal plane, self-excited oscillations can become very nonlinear [4–6]. They can saturate at an amplitude large with respect to the bunch size. The envelope of the synchrotron motion can also undergo very low frequency, large amplitude oscillations. Such self-excited motion, which oscillates between two different dynamic states, is referred to here as a relaxation oscillation. The relaxation frequency is orders of magnitude slower than the synchrotron frequency.

This paper presents experimental data taken from a detailed study of such relaxation oscillations, computer simulations that give further insights into the details of the oscillations, and an analytical model that describes the cyclic behavior of this nonlinear system. The instability studied is that commonly known as the coupled bunch instability. On the SPEAR electron storage ring, such an instability can be produced from a multitraversal effect acting on a single bunch. Most of the data presented in this paper were acquired in this case.

The bunch has qualitatively different characteristics at the different stages of its relaxation cycle. In the initial phase, at low amplitude, the bunch behaves as a single macroparticle that follows a harmonic oscillator equation. Its amplitude of oscillation grows toward an attractor at infinity. As the amplitude increases, nonlinearities manifest themselves through the reduction of the self-driving term and in the loss of charge density. These nonlinearities can account for the saturation of the amplitude, but a dynamic phase transition must occur in order for the system to enter its damping phase. During that phase transition, a new center of attraction appears. The single macroparticle model cannot explain this appearance, but a model including the flow of individual particles leaving the macroparticle can. Escaping particles lose synchronicity with the macroparticle and are therefore no longer driven by it. They then damp towards the origin. The rate of damping of the system is determined by the rate at which the current flows away from the macroparticle.

The macroparticle oscillation amplitude decreases, and the second center now accumulates charge and starts to grow. This second center now becomes the new macroparticle and the cycle is repeated. Models that use symmetric modes to describe this instability are inappropriate because of the observed asymmetry of the phase space distribution. This asymmetry starts with the growth as a macroparticle and continues throughout the cycle. For certain conditions of this self-interaction, the second macroparticle is visible at a fixed point approximately π out of phase with the first macroparticle. These phase-locked particles are also not symmetric.

II. EQUATION OF MOTION

A. Unperturbed oscillator

In electron storage rings, RF cavities are high Q resonant structures that provide the electric field necessary to compensate for the energy lost by the electrons. The energy gained by a particle in the RF cavity depends on its arrival time in the RF cavity. Its longitudinal phase space coordinates are (τ,δ), where τ is the delay and δ is the relative energy deviation of that particle with respect to the synchronous particle. The synchronous particle is the virtual particle that has energy E_0 and enters the cavity at $t=nT_0$, where T_0 is the revolution period of the machine. This particle loses an

amount of energy U_0 per turn, primarily from its emission of synchrotron radiation. The synchronous particle exactly recovers that amount of energy from the electric field in the RF cavity.

The evolution of the parameters (τ,δ) of a particle after one revolution of the ring from turn n to turn $n+1$ is given by

$$\tau_{n+1}=\tau_n+\alpha T_o\beta^2\delta_n, \tag{1}$$

$$\delta_{n+1}=\delta_n+\frac{eV_{rf}}{E_o}\sin(\varphi_s+\omega_{rf}\tau_{n+1})-\frac{U_o}{E_o}, \tag{2}$$

where α is the momentum compaction of the ring, β is the relativistic coefficient, very close to 1 for ultrarelativistic electrons, ω_{rf} is the RF angular frequency, and φ_s the synchronous phase defined by $U_0=eV_{RF}\sin\varphi_s$.

The phase is referenced to the zero crossing of sinusoidal voltage, and $\cos\varphi_s<0$. The variation over one turn can be replaced by a time derivative.

$$\dot{\delta}=\frac{\Delta\delta_n}{T_o}=\frac{eV_{rf}\sin(\varphi_s+\omega_{rf}\tau)-U_o}{E_oT_o}, \tag{3}$$

$$\dot{\tau}=\frac{\Delta\tau_n}{T_o}=\alpha\delta.$$

The equation of motion of a single particle can then be written as a second order differential equation

$$\ddot{\tau}=\frac{\alpha}{E_oT_o}[eV_{rf}\sin(\varphi_s+\omega_{rf}\tau)-U_o]. \tag{4}$$

For small amplitudes, this equation is that of a harmonic oscillator

$$\ddot{\tau}=-\omega_{so}^2\tau.$$

The natural synchrotron angular frequency ω_{so} is then defined by

$$\omega_{so}^2=\omega_o^2\frac{\alpha eV_{rf}h|\cos\varphi_s|}{2\pi E_o}.$$

In general, the motion is that of a circular pendulum. The frequency of oscillation is reduced quadratically with amplitude with respect to the natural synchrotron frequency. This amplitude dependence is of major importance in the description of the relaxation mechanism.

Since the particle energy loss per turn is itself energy dependent, the synchrotron motion is naturally damped. The equation of motion now has the form

$$\ddot{\tau}=\frac{\alpha}{E_oT_o}[eV_{rf}\sin(\varphi_s+\omega_{rf}\tau)-U_o]-2\alpha_{rad}\dot{\tau}, \tag{5}$$

with the radiation damping decrement

$$\alpha_{rad}=\frac{1}{2T_o}\left.\frac{dU_o}{dE}\right|_{E=E_o}.$$

B. Wake field

While passing through the RF cavity, the bunch can excite a high order mode (HOM in accelerator physics jargon). The electromagnetic fields produced by a particle can give longitudinal kicks to subsequent particles or incoming bunches, accelerating or decelerating them, depending on the phase of the field.

The potential generated by a unit particle is commonly referred to as a wake potential, or wake field. Wake fields from HOMs can be represented by the impulse response of a comparable electrical circuit, consisting of a parallel combination of a resistor (R), an inductor (L), and a capacitor (C), known as an RLC circuit. The wake field generated at time τ and observed at time t, due to a HOM whose characteristics are R_s,α_R,f_R, is given by [7]

$$W(t-\tau)=2\alpha_RR_sU(t-\tau)e^{-\alpha_R(t-\tau)}\left\{\cos[\bar{\omega}(t-\tau)]-\frac{\alpha_R}{\bar{\omega}}\sin[\bar{\omega}(t-\tau)]\right\}, \tag{6}$$

with

$$U(t)=\begin{cases}1 & t>0\\ 1/2 & t=0\\ 0 & t<0\end{cases}$$

and

$$\bar{\omega}=\sqrt{\omega_R^2-\alpha_R^2}.$$

R_s is the shunt resistance (10 MΩ in this study), α_R is the damping rate of the HOM related to the quality factor Q by $\alpha_R=\omega_R/2Q$ (Q is 20 000 in this study), and f_R is the resonant frequency (358 MHz in this study). The length of the cavity is much smaller than the circumference of the ring and can be assumed to be pointlike. The retarding voltage $V(\tau)$ induced by a bunch containing N particles of charge e is $NeW(\tau)$.

This term adds a perturbing driving force to the harmonic oscillator equation. Equation (5) becomes

$$\ddot{\tau}+2\alpha_{rad}\dot{\tau}-\frac{\alpha}{E_oT_o}[eV_{rf}\sin(\varphi_s+\omega_{rf}\tau)-U_o]=-\frac{\alpha NeW(\tau)}{E_oT_o}. \tag{7}$$

III. EXPERIMENT RESULTS

A. Motivations

Small dimensions and stability of the bunch in time and energy are essential for high performance of storage rings, for both collider rings and synchrotron radiation sources. Particles are lost from the accelerator when the amplitudes of their synchrotron oscillations exceed the acceptance of the machine.

The voltage induced by the beam on the cavity impedance, at the upper synchrotron sideband of the revolution harmonics, has a destabilizing effect on the beam. This in-

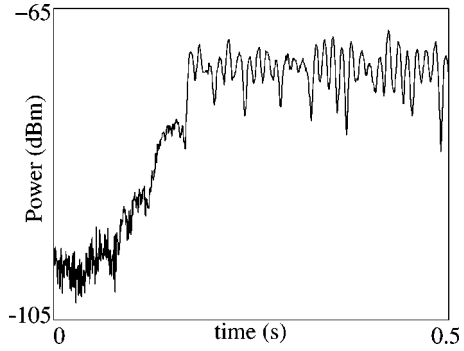

FIG. 1. Spectrum analyzer zero-span output for the cavity signal at $751f_0+f_s$. The first 0.2 seconds of the scan show the amplitude at the onset of an unstable synchrotron oscillation. The rest shows the low frequency relaxation oscillation about the saturation level.

stability, commonly known as the coupled bunch instability, occurs when this force exceeds the net damping force.

While characterizing the RF cavities in order to improve the stability of SPEAR [8], much of our attention was paid to the growth of the HOM-induced instabilities. A regular modulation about the saturation level was observed (Fig. 1) [9]. Its period is always longer than a radiation damping time. This modulation is often small, but certain machine parameters can make it very large, regular, and quite striking (Fig. 2). The possibility of adjusting the HOM frequency by positioning a moveable RF cavity tuner in the passive RF cavity made such observations very repeatable and convenient to study on the SPEAR ring.

B. Time scales

The experimental parameters are presented in Table I. At 2.3 GeV, the natural radiation damping time is 10 ms, but the total damping time was measured to be 5 ms (at 2 mA). This figure was used for the analysis. The resonance studied is the fundamental resonance, $f_{HOM}=f_{RF}$. (Improper tuning of the fundamental resonance, as studied here, in a powered RF cavity results in the instability known as the Robinson instability [10].) The large variety of time scales involved in the relaxation mechanism is presented in Table II.

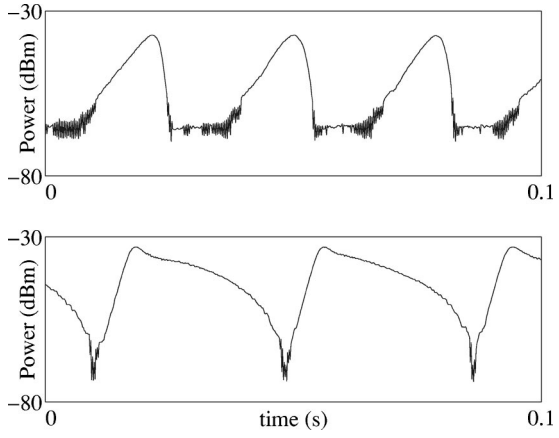

FIG. 2. Spectrum analyzer zero-span output for the cavity signal at $f_{HOM}+f_s$. Data such as these were fit, as a function of f_{HOM}, for frequency, maximum and minimum oscillation power, growth times, and damping times.

TABLE I. Machine parameters.

Energy	U_0	V_{RF}	τ_{damp}	R_S
2.3 GeV	193 keV	1.68 MV	5 ms	10 MΩ

The wide range of these time scales means that these phenomena occupy different ranges of the frequency spectrum. Discrete series can be approximated by continuous integrals. Synchrotron oscillations can be averaged to give simplified equations of motion for the relaxation oscillation.

C. Description of measurements

Since the amplitude of the driving force depends on the HOM strength, the largest RF cavity impedance was chosen for the study. SPEAR has two RF cavities, but needs only one powered for normal operation. Therefore, the largest available impedance is the fundamental mode of the idle RF cavity. The HOM impedance produces a strong long-range wake field at currents for which the short-range effects of the total ring impedance can be neglected.

Liberty has been taken with the term HOM in this paper. In all storage rings, the fundamental cavity mode is tuned to be stable, and stability problems from narrow band impedances come only from true HOMs. But the physics of the instability depends only on the characterisitcs of the resonator; it does not depend on whether the mode is the fundamental or of higher order. In this paper, HOM will also refer to the fundamental mode in the idle cavity.

The independent variables in the study are machine current, energy, and HOM center frequency. Of those three, the HOM center frequency has the most striking effect on the dynamics of the problem. This frequency can be accurately tuned by positioning a movable RF cavity tuner.

1. Spectrum analyzer

The first series of data were taken on an RF spectrum analyzer and downloaded via a GPIB program to a PC for data analysis. (All software for data collection, analysis, and simulation is a combination of codes written internally at SSRL in the C programming language and MATLAB© [11].) The signal came from a probe in the RF cavity. The spectrum analyzer was used as a narrow-band receiver, in zero-span mode, tuned on the upper synchrotron sideband of the fundamental RF harmonic. Its resolution bandwidth, 10 kHz, allowed reasonable rejection of the RF harmonic while preserving the ability to see fast dynamic changes in the amplitude of the sideband. In particular, the value of the synchrotron frequency varies by several kHz over a relaxation cycle.

TABLE II. System time scales.

	Frequency	Period	N_{turns}
$f_{sawtooth}$	<100 Hz	>10 ms	$>12\,800$
f_{so}	28.4 kHz	35 μs	45
α_R	56 kHz	17.8 μs	23
f_o	1.28 MHz	0.78 μs	1
$f_{RF}=f_{HOM}$	358.5 MHz	2.8 μs	1/280
$(1/\sigma_\tau)$	10 GHz	100 ps	1/7840

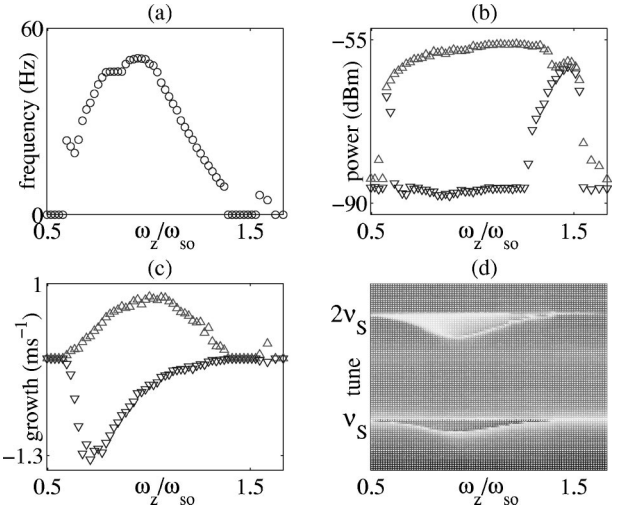

FIG. 3. Relaxation oscillation parameters vs f_{HOM}: (a) relaxation oscillation frequency, (b) maximum ($\triangle$) and minimum ($\triangledown$) powers of oscillation, (c) growth times ($\triangle$) and damping times ($\triangledown$), (d) ν_s, showing $\sim$15% deviation over the range of f_{HOM}.

The evolution of crucial parameters of the relaxation oscillation as a function of the resonator frequency is summarized in Fig. 3. From the amplitude information, one sees that, at the instability threshold, the amplitude of the oscillation quickly reaches its saturation value. Beyond that threshold, the maximum amplitude does not significantly increase, but the large amplitude relaxation oscillations start almost immediately. The growth rate, as a function of frequency, is symmetric with respect to the center frequency. It matches the resistive part of the resonator impedance. The damping rate is not nearly as symmetric. It is very small over the second half of the resonance curve [Fig. 3(c)]. Because of this asymmetry, the frequency of the relaxation oscillation as a function of the HOM frequency is also asymmetric.

The variation and/or spread of the synchrotron tune during these oscillations was also measured. These data were obtained by frequency demodulating a signal from a pickup in the storage ring. The demodulated signal was then input into a digital spectrum analyzer. Since the analyzer averaged over many relaxation periods, this measurement could not resolve the difference between a tune variation and a spread of tune within the bunch over the oscillation. The frequency deviation showed a decrease of 15% from the nominal synchrotron frequency, corresponding to the shift for large amplitude pendulum oscillations [Fig. 3(d)].

2. Streak camera

All of the spectrum analyzer data only give information about the dipole moment of the beam. The next set of data was taken with a streak camera, an instrument that gives information about the internal structure of the beam. Previous attempts to explain these oscillations have used mode coupling techniques [12,13], but the streak camera images show that this technique is not appropriate for compactly describing this behavior. The great advantage of using a streak camera was that the data obtained gave us key clues with which to build a simple and accurate model.

Synchrotron radiation emitted by the electron beam in the dipole is the incident signal to the streak camera. A photocathode in the camera transforms the time-dependent radiation into a beam of electrons, which are then rotated by an angle of 90° inside the camera before striking a photoanode. The photoanode re-emits photons that are then imaged on the camera's charge-coupled-device (CCD) array. This rotation transforms the longitudinal temporal distribution of the bunch into a vertical photon distribution (or ''streak'') which can be read out of the camera (Fig. 4). The streak camera data were taken with the same machine parameters as the spectrum analyzer data. Again, the resonator frequency was the main independent variable. Data were taken both at a slow scan rate, one slow enough to see the entire relaxation oscillation cycle, and at a fast rate, one short enough to see a single streak every third revolution period.

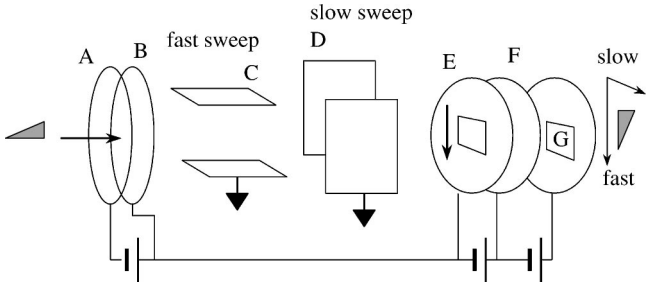

FIG. 4. Schematic diagram of a dual sweep streak camera. *A*, photocathode; *B*, accelerating mesh; *C*, vertical sweep plates; *D*, horizontal sweep plates; *E*, microchannel plate; *F*, phosphor screen; *G*, CCD camera.

On the slow scan range, the entire relaxation oscillation cycle was captured. While growing, the envelope visible in the slow scan shows the bunch to be concentrated near the extremes of the oscillation. But its charge density decreases with time [Fig. 5(a)]. The maximum amplitude of oscillation reached is about $\pi/2$ radians. In the damping phase, this macroparticle still exists and damps, but it has a much reduced intensity compared to its initial value. At the end of this phase, particles have accumulated around the center. In the particular case of f_{HOM} slightly above hf_0+f_{so}, when the damping is very slow, a second accumulation point clearly forms near the origin [Fig. 5 (b)]. The charge at this point grows in both amplitude and intensity as the original macroparticle continues its decay.

The slow data confirm the periodic nature of the phenomenon and allow fast scan data to be taken and correctly interpreted. These data show the distribution of the bunch at every third turn, so that many distinct images are displayed

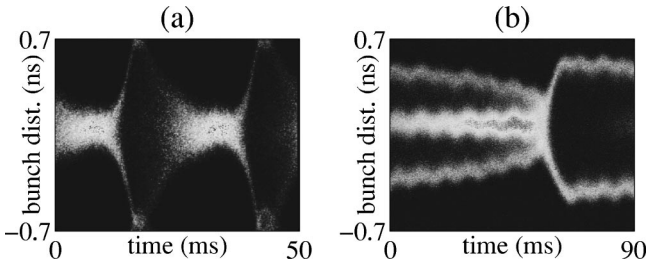

FIG. 5. Relaxation cycles for two different values of f_{HOM}: (a) $f_z \sim f_s$, (b) $f_z > f_s$, showing the appearance of a second center, accumulation of particles there, and its growth. Note that (b) has much slower damping than (a).

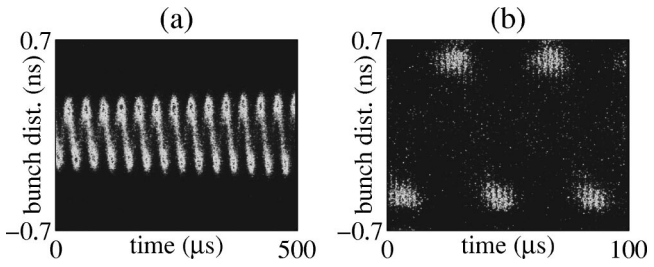

FIG. 6. (a) Growth of bunch as a macroparticle; (b) saturation of main body with signs of filamentation visible.

along each synchrotron oscillation period. By comparing the envelope of these images with that of the slow scan images, the proper stage in the relaxation cycle can be identified. These data show that the bunch behaves as a single macroparticle during its growth, oscillating between extremes and slowly losing particles (Fig. 6). The second accumulation point, when seen, is phase-locked to the initial macroparticle, but approximately π out of phase with it (Fig. 7). It stays locked with the macroparticle and grows in amplitude, as the original macroparticle damps. These streak camera images clearly show the two dynamic phases of the system. One center grows exponentially, then saturates [Figs. 5 and 6(b)]. It continues to lose particles, which accumulate at a second center. The second center grows in amplitude as it accumulates more particles. Meanwhile, the first center damps. The two centers have now exchanged roles in this oscillation, giving the system a bistable character.

IV. SIMULATIONS

A. Simulation program

Since the streak camera images show a loss and an asymmetric variation of charge density, a multiparticle simulation program was written to determine the evolution of the bunch phase space distribution, turn after turn, in the presence of a perturbing long term wake field. Individual particles obey a second order difference equation with a driving force proportional to the wake term $W(\tau)$ of Eq. (6). The driving force is the combination of the wake field generated by particles ahead of it in the same bunch, and of all the wake fields generated from each particle on all previous turns.

The turn-by-turn difference equation of the code includes the synchrotron radiation emission through losses, radiation damping, and quantum fluctuations. The long memory of the high Q cavity is retained by the use of propagators. They enable the accurate retention of the phase information of the rapidly oscillating wake over the comparatively long time scale of one revolution period. To get more than an entire relaxation cycle, 10^5 turns were commonly computed for a population of 20 000 particles, distributed over 300×300 cells covering the area spanned by the 2π size of the RF bucket and ±20 standard deviations of the natural energy spread. Each run calculating one second of evolution of the distribution of 20 000 particles takes only a few hours on a standard PC. Details on the wake field computation are presented in the Appendix.

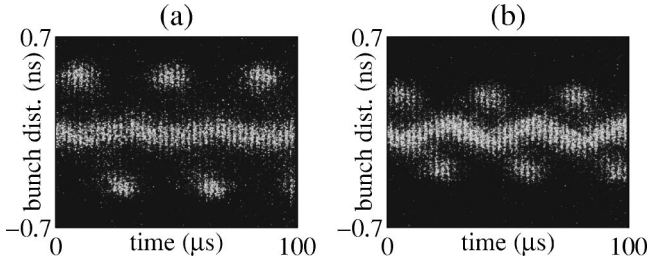

FIG. 7. Two centers during damping for $f_z>f_s$, with individual streaks now visible. (a) The second center has more charge than the original main body, yet its oscillation amplitude is still small. (b) The second center now has most of the charge. Its amplitude continues to grow while that of the original main body continues to damp. Oscillations are about π out of phase.

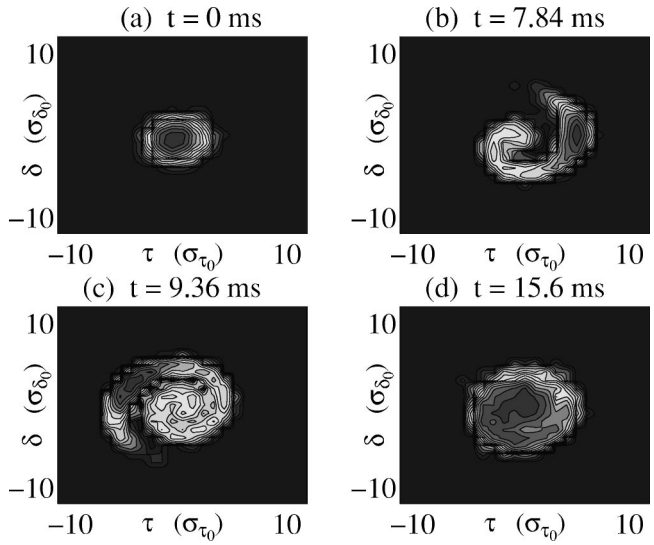

FIG. 8. Distribution in phase space (charge density levels are plotted in a logarithmic scale). (a) Beginning of the relaxation oscillation cycle; (b) initial growth: the bunch starts to filament; particles leave the head of the bunch (gain $\Delta\bar{\phi}>0$ with respect to the main body); (c) filamentation: the escaping particles spiral toward the center (second attractor) while the main body reaches its limit cycle; (d) damping: the bunch has lost its initial charge density distribution and damps.

B. Simulation results

The results of the simulations are in good agreement with experimental results. They reproduce the very low frequency of the relaxation oscillation (always below 100 Hz in our case). They confirm qualitatively the evolution of frequency and amplitude as a function of the induced voltage. These simulations reproduce the $\pi/2$ limit cycle amplitude observed with the streak camera. Finally, the simulations corroborate the streak camera data, discussed above, that show that the bunch grows as a macroparticle that loses charge density to an attractor at the center (Fig. 8).

Based on these results, the predictions of the simulations could be viewed with confidence. They were used to gain further insight into the details of the oscillation too sensitive to be seen with our experimental setup. The tracking code phase space distribution shows that the filamentation starts from the head of the bunch. Particles spiral from the head of the bunch towards the center of phase space [Fig. 8(b)]. One can observe that these particles perform synchrotron oscillations at a higher frequency than those still attached to the

main body. These results gave important clues for the theoretical model.

Additional comparisons such as formation of the second stable fixed point when f_{HOM} is slightly above pf_0+f_{so} remain to be studied.

V. ANALYTICAL MODEL

A. Introduction

A simple analytical model of this system, explaining the main features of the experimental data and simulations, has been developed. It takes advantage of the greatly different time scales of the mechanism. The series of discrete, impulsive forces on the system are approximated by a continuous expression, allowing a closed form solution of the equations of motion to be developed. Another simplification can be made because of the slowly varying changes of the oscillation amplitude and frequency with respect to the synchrotron oscillation frequency. The expression of the driving force presented here reduces to a single infinite sum that rapidly converges. The two-particle version of this model reproduces the main characteristics of the system.

B. Continuous approximation

As given in Sec. II B, the impedance of the cavity resonance can be modeled as a resonator with a wake function (potential per unit charge) acting at time t and due to a source particle present at time τ,

$$W(t-\tau)=U(t-\tau)2\alpha_R R_S e^{-\alpha_R(t-\tau)}\cos[\omega_R(t-\tau)+\phi_R].$$

The total wake can then be represented by an infinite sum of wakes generated during previous traversals of the cavity. The decelerating wake potential seen at time t is then

$$W(t)=2\alpha_R R_S\sum_{u=-\infty}^{t} e^{-\alpha_R(t-u)}\cos[\omega_R(t-u)],$$

where $\alpha_R\equiv\omega_R/2Q$. If the bunch revolution period were constant at T_0, t would be replaced by nT_0, u would be replaced by kT_0, and the wake potential would be

$$W(nT_0)=2\alpha_R R_S\sum_{k=-\infty}^{n} e^{-\alpha_R(n-k)T_0}\cos[\omega_R(n-k)T_0].$$

Since the revolution period is almost, but not exactly, constant, in order to keep the physics of the equation, one needs to keep a term, small compared to T_0, that represents the variation of arrival time. Therefore,

$$t=nT_0+\tau_n,$$

$$u=kT_0+\tau_k.$$

Now

$$W(t)=2\alpha_R R_S\sum_{k=-\infty}^{n} e^{-\alpha_R[(n-k)T_0+(\tau_n-\tau_k)]}\times\cos\{\omega_R[(n-k)T_0+(\tau_n-\tau_k)]\}.$$

Representing $\omega_R=p\omega_0+\omega_z$ as an integral multiple and a fractional part of the revolution harmonic, the sum becomes

$$\begin{aligned}W(t)&=2\alpha_R R_S\sum_{k=-\infty}^{n} e^{-\alpha_R[(n-k)T_0+(\tau_n-\tau_k)]}\cos\{(p\omega_0+\omega_z)[(n-k)T_0+(\tau_n-\tau_k)]\}\\&=2\alpha_R R_S\sum_{k=-\infty}^{n} e^{-\alpha_R[(n-k)T_0+(\tau_n-\tau_k)]}\cos[p(n-k)\omega_0T_0+\omega_z(n-k)T_0+\omega_R(\tau_n-\tau_k)]\\&\approx 2\alpha_R R_S\sum_{k=-\infty}^{n} e^{-\alpha_R(n-k)T_0}\cos[\omega_z(n-k)T_0+\omega_R(\tau_n-\tau_k)],\end{aligned}$$

where in the last line the small difference in the monotonic damping due to the deviations of the revolution period have been ignored and multiples of 2π have been removed from the argument of the cosine term. Using the representations $t=nT_0$, $u=kT_0$, $\tau_n=\tau(nT_0)$, $\tau_k=\tau(kT_0)$, and the identity $1\equiv(1/T_0)\int_{(k-1)T_0}^{kT_0}du$, the time-dependent part of the wake can be represented by the continuous convolution integral

$$\begin{aligned}W(t)&=2\alpha_R R_S\sum_{k=-\infty}^{n}\frac{1}{T_0}\int_{(k-1)T_0}^{kT_0} e^{-\alpha_R(n-k)T_0}\cos[\omega_z(n-k)T_0+\omega_R(\tau_n-\tau_k)]du\\&=2\alpha_R R_S\frac{1}{T_0}\int_{-\infty}^{t} e^{-\alpha_R(t-u)}\cos\{\omega_z(t-u)+\omega_R[\tau(t)-\tau(u)]\}du.\end{aligned}$$

When the bunch has N particles of charge e, the electrical potential $V(t)$ generated by the wake is

$$\begin{aligned}V(t)&=2\alpha_R R_S\frac{1}{T_0}\int_{-\infty}^{t}(Ne)e^{-\alpha_R(t-u)}\cos\{\omega_z(t-u)+\omega_R[\tau(t)-\tau(u)]\}du\\&=2\alpha_R R_S\int_{-\infty}^{t} Ie^{-\alpha_R(t-u)}\cos\{\omega_z(t-u)+\omega_R[\tau(t)-\tau(u)]\}du,\end{aligned}$$

where I is the current in the bunch.

C. Evaluation of the integral

The continuous approximation of the synchrotron motion is that of common pendulum motion. Even for large amplitude oscillations observed in these data, the motion is still very close to sinusoidal. $\tau(t)$ and $\tau(u)$ can be represented as slowly varying sinusoidal functions

$$\tau_t(t)=\hat{\tau}_t\cos(\omega_{st}t+\phi_t),$$

$$\tau_u(t)=\hat{\tau}_u\cos(\omega_{su}t+\phi_u),$$

since $\hat{\tau}_t$, $\hat{\tau}_u$, ω_{st}, ω_{su}, ϕ_t, and ϕ_u are all slowly varying functions of time with respect to the synchrotron frequency. The integral $V(t)$ can then be explicitly computed. Even though the integral starts at $-\infty$, the exponential damping of the HOM means that the only important contributions come from times no further back than a few resonator damping times. For this system, this resonator damping time is also comparable to the synchrotron period so that with the slowly varying approximation, $\hat{\tau}_u$, ω_{su}, and ϕ_u can be considered as constants in the integration.

The potential term can be expressed as

$$\begin{aligned}V(t)&=2\alpha_R R_S I\int_{-\infty}^{t}e^{-\alpha_R(t-u)}\cos[\omega_z(t-u)+\omega_R(\tau_t-\tau_u)]du\\&=2\alpha_R R_S I\,\mathrm{Re}\left\{\int_{-\infty}^{t}e^{-\alpha_R(t-u)}e^{j[\omega_z(t-u)+\omega_R(\tau_t-\tau_u)]}du\right\}\\&=2\alpha_R R_S I\,\mathrm{Re}\left\{e^{-\alpha_r t+j[\omega_z t+\hat{\tau}\omega_R\cos(\omega_{st}t+\phi_t)]}\int_{-\infty}^{t}e^{\alpha_r u-j\omega_z u}e^{-j\hat{\tau}_u\omega_R\cos(\omega_{su}u+\phi_u)}du\right\}.\end{aligned}$$

Using the expansion

$$e^{j\hat{\tau}\omega_R\cos(\omega_s u+\Psi)}=\sum_{m=-\infty}^{\infty}j^m J_m(\hat{\tau}\omega_R)e^{jm(\omega_s u+\Psi)}$$

and the notation $r_t=\hat{\tau}_t\omega_R$ and $r_u=\hat{\tau}_u\omega_R$, this integral can be expressed as the doubly infinite sum

$$V(t)=2\alpha_R R_S I\,\mathrm{Re}\left\{\sum_{p,m=-\infty}^{\infty}\frac{j^{p-m}J_p(r_t)J_m(r_u)e^{j(p\omega_{st}+m\omega_{su})t}e^{jp\phi_t+jm\phi_u}}{\alpha_r+j(m\omega_{su}-\omega_z)}\right\}. \tag{8}$$

D. KBM method

The averaging method of Krylov, Bogoliubov, and Mitropolsky [14–16] is well suited to such an oscillatory problem with slowly varying parameters [17]. To solve a driven harmonic oscillator

$$\ddot{x}+\omega_{s_0}^2 x=f_x(x,\dot{x}),$$

new variables (r,ϕ) are defined in terms of $(x,\dot{x})$ by the equations

$$x=r(t)\cos[\omega_{s_0}t+\phi(t)],$$

$$\dot{x}=-\omega_{s_0}r(t)\sin[\omega_{s_0}t+\phi(t)].$$

By equating

$$\dot{x}=\frac{dx}{dt},$$

$$\ddot{x}=\frac{d\dot{x}}{dt},$$

one obtains the differential equations for the amplitude and phase of the oscillation,

$$\dot{r}=-\frac{1}{\omega_{s_0}}\sin(\omega_{s_0}t+\phi)f(r,\phi),$$

$$\dot{\phi}=-\frac{1}{\omega_{s_0}r}\cos(\omega_{s_0}t+\phi)f(r,\phi),$$

where $f(r,\phi)$ is the driving force expressed in terms of (r,ϕ). The Krylov-Bogoliubov-Mitropolsky (KBM) approximation involves taking the average value of the force over the period of oscillation. Denoting the time-averaged values of r and ϕ by $\bar{r}$ and $\bar{\phi}$, respectively, the desired equations of motion are

$$\dot{\bar{r}}=-\frac{1}{2\pi}\int_{t-(2\pi/\omega_{s_0})}^{t}\sin(\omega_{s_0}\tau+\phi)f(r,\phi)d\tau, \tag{9}$$

$$\dot{\bar{\phi}}=-\frac{1}{2\pi r}\int_{t-(2\pi/\omega_{s_0})}^{t}\cos(\omega_{s_0}\tau+\phi)f(r,\phi)d\tau. \tag{10}$$

If $f(r,\phi)$ is expanded in a Fourier series with respect to the oscillation frequency ω_{s_0},

$$f(r,\phi)=F_0(r,\phi)+\sum_{n=1}^{\infty}\left[F_{Cn}(r,\phi)\cos(n\omega_{s_0}t+\phi)\right.$$
$$\left.+F_{Sn}(r,\phi)\sin(n\omega_{s_0}t+\phi)\right], \tag{11}$$

then the averaged evolution equations of the oscillation amplitude and phase become

$$\dot{\bar{r}}=-\frac{1}{2\omega_{s_0}}F_{S1}(\bar{r},\bar{\phi}),$$

$$\dot{\bar{\phi}}=-\frac{1}{2\omega_{s_0}\bar{r}}F_{C1}(\bar{r},\bar{\phi}).$$

E. Application of the KBM method

The evolution of the amplitude and frequency of the synchrotron oscillation due to the wake field force can now be extracted from Eq. (8). Contributions to F_{S1} and F_{C1} will only occur when $p=-m\pm1$. After some algebra, one obtains the Fourier coefficients of $\sin(\omega_{st}t+\phi_t)$ and $\cos(\omega_{st}t+\phi_t)$, respectively, as

$$F_{S1}=-\frac{\omega_{s_0}^2}{V_{RF}|\cos\varphi_s|}2\alpha_R R_S I\sum_{m=1}^{\infty}J_m(r_u)[J_{m-1}(r_t)+J_{m+1}(r_t)]\left\{\left[\frac{\alpha_R}{\alpha_R^2+(m\omega_{su}-\omega_z)^2}-\frac{\alpha_R}{\alpha_R^2+(m\omega_{su}+\omega_z)^2}\right]\cos(m\Delta\phi)\right.$$
$$\left.-\left[\frac{(m\omega_{su}-\omega_z)}{\alpha_R^2+(m\omega_{su}-\omega_z)^2}-\frac{(m\omega_{su}+\omega_z)}{\alpha_R^2+(m\omega_{su}+\omega_z)^2}\right]\sin(m\Delta\phi)\right\}, \tag{12}$$

$$F_{C1}=\frac{\omega_{s_0}^2}{V_{RF}|\cos\varphi_s|}2\alpha_R R_S I\left\{2\frac{\omega_z}{\alpha_R^2+\omega_z^2}J_0(r_u)J_1(r_t)+\sum_{m=1}^{\infty}J_m(r_u)[J_{m-1}(r_t)-J_{m+1}(r_t)]\right.$$
$$\times\left[\left(\frac{(m\omega_{su}-\omega_z)}{\alpha_R^2+(m\omega_{su}-\omega_z)^2}-\frac{(m\omega_{su}+\omega_z)}{\alpha_R^2+(m\omega_{su}+\omega_z)^2}\right)\cos(m\Delta\phi)\right.$$
$$\left.\left.+\left(\frac{\alpha_R}{\alpha_R^2+(m\omega_{su}-\omega_z)^2}-\frac{\alpha_R}{\alpha_R^2+(m\omega_{su}+\omega_z)^2}\right)\sin(m\Delta\phi)\right]\right\}, \tag{13}$$

where $\Delta\phi=\phi_t-\phi_u$. These terms describe the force on a test particle t due to a macroparticle u carrying current I. This paper concentrates on a two-particle model. To generalize to a distribution, the total force on a particle at (r_t,ϕ_t) is calculated from the integral of the forces generated by particles distributed in (r_u,ϕ_u) and weighted by their charge.

The wake field is not the only effect that must be included to describe the behavior of this system. The radiation damping can be considered constant over the energy range of interest. The radiation damping term contributes only to the $\dot{\bar{r}}$ equation. The pendulum frequency decreases with increasing amplitude. To first order, this decrease can be approximated by a term quadratic in r [16]. Since these terms all satisfy the slowly varying approximations, the KBM method can be applied by treating the three terms as independent contributions to the equations of motion of $\bar{r}$ and $\bar{\phi}$.

The final, averaged equations of motion for a test particle at (r_t,ϕ_t) due to a macroparticle at (r_u,ϕ_u) are

$$\dot{\bar{r}}_t=-\frac{1}{2\omega_{st}}F_{S1}(\bar{r}_t,\bar{\phi}_t,\bar{r}_u,\bar{\phi}_u)-\alpha_{rad.}\bar{r}_t, \tag{14}$$

$$\dot{\bar{\phi}}_t=-\frac{1}{2\omega_{st}\bar{r}_t}F_{C1}(\bar{r}_t,\bar{\phi}_t,\bar{r}_u,\bar{\phi}_u)-\frac{1}{16}\bar{r}_t^2\omega_{st}. \tag{15}$$

VI. ANALYSIS OF RELAXATION OSCILLATIONS

A. Description of equations of motion

Equations (14) and (15) contain the key features of the dynamics of the system. These equations are expressed in a rotating coordinate system in which the source particle moves radially along the $\phi=0$ axis. The angular position of the test particle is given by its deviation in phase, $\Delta\phi$, from the source. For small and slowly varying differences in the frequencies of the two particles, $\Delta\phi\approx(\omega_{st}-\omega_{su})t$. One term that affects the frequency of the test particle in Eq. (13) is independent of ϕ. All other terms have a harmonic dependence on it and average to zero as the test particle rotates by 2π. In particular, the growth generated by the wake field on a test particle with a synchrotron frequency different from that of the source is nearly zero.

For amplitudes of r within the RF bucket size, the Bessel coefficients make the infinite series in Eqs. (12) and (13) converge rapidly. When the impedance is such that $\omega_z=\omega_{su}$, the dominant terms in those equations are the coefficients of $\cos(m\Delta\phi)$ and $\sin(m\Delta\phi)$, respectively. Consequently, these terms have a similar distribution in this coordinate system, but one is rotated by $\pi/2$ with respect to the other. In this case, the line of maximal growth and the line of zero frequency shift both lie near $\Delta\phi=0$.

For the case of a single macroparticle model, $r_t=r_u$ and $\Delta\phi=0$. Each term of Eqs. (12) and (13) are antisymmetric under the interchange of $(m\omega_{su}-\omega_z)$ with $(m\omega_{su}+\omega_z)$.

This shows that tuning the resonance from an upper ($\omega_z = +\omega_s$) to a lower ($\omega_z = -\omega_s$) synchrotron sideband changes a growth rate to a damping rate of the same magnitude. This general result confirms the well known property first reported by Robinson [10]. In most cases, the $m=0$ and $m=1$ terms of the series give a good approximation to the total sum:

$$F_{S1\approx} = -\frac{\omega_{s_0}^2}{V_{RF}|\cos\varphi_s|} 2\alpha_R R_S I J_1(r_u)[J_o(r_t)+J_2(r_t)] \times\left[\frac{\alpha_R}{\alpha_R^2+(\omega_{su}-\omega_z)^2}-\frac{\alpha_R}{\alpha_R^2+(\omega_{su}+\omega_z)^2}\right],$$

$$F_{C1\approx} = \frac{\omega_{s_0}^2}{V_{RF}|\cos\varphi_s|} 2\alpha_R R_S I\left\{2\frac{\omega_z}{\alpha_R^2+\omega_z^2}J_0(r_u)J_1(r_t) + J_1(r_u)[J_o(r_t)-J_2(r_t)]\left[\frac{(\omega_{su}-\omega_z)}{\alpha_R^2+(\omega_{su}-\omega_z)^2} - \frac{(\omega_{su}+\omega_z)}{\alpha_R^2+(\omega_{su}+\omega_z)^2}\right]\right\}.$$

B. Linear regime

Using the narrow-band resonator impedance approximation

$$Z(\omega_R+\Delta\omega) = \alpha_R R_S \frac{\alpha_R + j\Delta\omega}{\alpha_R^2+\Delta\omega^2}$$

and the small amplitude expansion of the Bessel functions, one recovers the formulas for growth and frequency shifts given in [18,7]:

$$\dot{\bar{r}} = \frac{\omega_{s_0}}{2V_{RF}|\cos\varphi_s|} I\,\mathrm{Re}\{Z(h\omega_0+\omega_{s_0}) - Z(h\omega_0-\omega_{s_0})\}\bar{r} - \alpha_{rad}\bar{r},$$

$$\dot{\bar{\phi}} = \frac{\omega_{s_0}}{2V_{RF}|\cos\varphi_s|} I\,\mathrm{Im}\{2Z(h\omega_0) - Z(h\omega_0+\omega_{s_0}) - Z(h\omega_0-\omega_{s_0})\}.$$

When $\mathrm{Re}\{Z(h\omega_0+\omega_{s_0})-Z(h\omega_0-\omega_{s_0})\}$ is sufficiently large, the bunch amplitude grows toward an attractor at infinity.

C. Growth as a macroparticle

A bunch has Gaussian distributions along the two dimensions of the phase space. Its thermal distribution is the result of an equilibrium between quantum excitation and radiation damping. But despite its finite dimensions, the bunch can be treated as a macroparticle, since it keeps its cohesion during the first stage of its growth. This property can be deduced from the representations of Eqs. (12) and (13) in Fig. 9. These equations give the expression of the driving force acting on a test particle located at $(r_t, \Delta\phi)$ and produced by the main body, or source, located at $(r_u, \Delta\phi = 0)$. For convenience in expansions around the main body, Δr is defined as $\Delta r = r_t - r_u$.

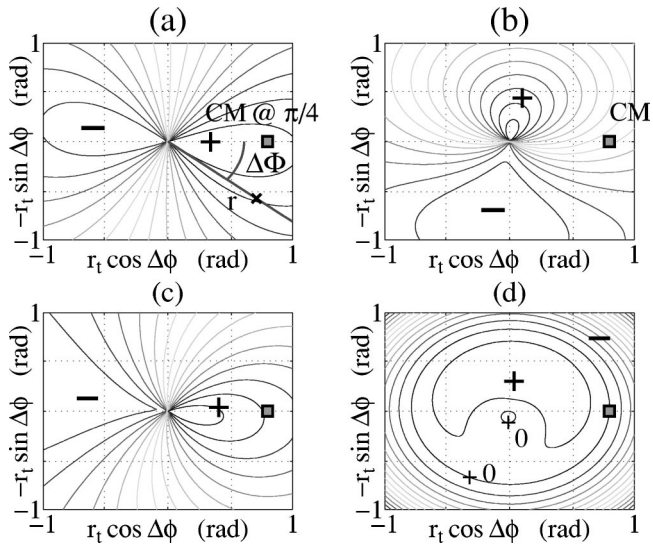

FIG. 9. Amplitude of $\dot{\bar{r}}$ and $\dot{\bar{\phi}}$ in rotating phase space. The main body, or center of mass (CM) at ($r_u = \pi/4$, $\phi_u = 0$) contains all of the charge; the test particle at $(\bar{r_t}, \bar{\phi_t})$ has negligible charge; $\omega_z = \omega_{so}$. (a) Wake field component in quadrature with oscillation and proportional to the $F_{S1}(\bar{r_t}, \bar{\phi_t})$ function; particles in the (+) region are strongly driven by the force generated by the CM; particles in the (−) region are damped. (b) Wake field component in phase with the synchrotron motion of the CM and proportional to $F_{C1}(\bar{r_t}, \bar{\phi_t})$; particles in the (+) region undergo an increase in synchrotron frequency, ω_{st}, ($\Delta\dot{\bar{\phi}} > 0$); particles in the (−) region undergo a decrease ($\Delta\dot{\bar{\phi}} < 0$). (c) Same as (a), but includes the radiation damping term ($-\alpha_{rad}\bar{r_t}$); the region of damping now extends over a wider zone. (d) Same as (b) but includes the pendulum frequency shift; the pendulum frequency shift (which reduces ω_{st} with increasing radial amplitude) dominates at large amplitudes ($\bar{r_u} > 0.2$ radians).

In Fig. 9(b), the representation of the frequency shift induced by the macroparticle wake shows that (1) particles delayed with respect to the main body ($\Delta\phi < 0$) will experience a greater $\dot{\bar{\phi}}$ than the main body and will therefore catch up to it, and (2) particles ahead of the main body will be decelerated ($\Delta\dot{\bar{\phi}} < 0$) and will fall back to it. The wake field induced frequency shift provides an azimuthal attracting force.

In Fig. 9(a), the representation of the growth rate induced by the macroparticle wake shows that (1) particles with $\Delta r < 0$ and $\Delta\phi = 0$ will see more growth than the main body and will be drawn out to it, and (2) particles with $\Delta r > 0$ and $\Delta\phi = 0$ will see less growth than the main body and will be drawn back to it.

In conclusion, the main body is an attractor for all the particles of the bunch.

D. Filamentation

Until now, the pendulum frequency shift was negligible compared to the shift induced by the wake field. In the experiment performed on SPEAR, with the parameters de-

scribed in Table I, the position of the bunch at which the pendulum frequency shift starts to dominate that induced by the wake is at $\tau=0.2$ radians, for particles at $\Delta\phi=0$. At these amplitudes, the quadratic radial dependency of the pendulum frequency shift causes an asymmetry in Δr that allows the test particle to escape from the front of the bunch.

(1) Particles with ($\Delta r=0$, $\Delta\phi>0$) and ($\Delta r=0$, $\Delta\phi<0$) will undergo the same growth as the main body, and will tend to get pulled back towards it as during the early stage of growth. As before, the wake field induced frequency shift provides an azimuthal attracting force.

(2) A particle with ($\Delta r>0$, $\Delta\phi=0$) will experience a larger pendulum frequency shift than the main body and acquire a $\Delta\phi<0$. This shift in angle leads it to a region of smaller radial growth, decreasing Δr, and therefore of increasing synchrotron frequency. This sequence of events will lead it back to the main body.

(3) A particle with ($\Delta r<0$, $\Delta\phi=0$) will experience a smaller frequency shift, due to the pendulum effect, than that induced by the wake field from the main body. Since the pendulum term now dominates over the wake field term, the test particle acquires a $\Delta\phi>0$. Because the main bunch is near the angle of maximum growth, the test particle at positive $\Delta\phi$ also sees a driving force smaller than that seen by the main body and so moves even further away from it radially, intensifying the pendulum effect. The particle will therefore escape from the front of the main body.

The escape of particles from the head of the bunch and compression of particles at the tail of the bunch is exactly what is observed with the tracking code. The loss of density of the main body is also in good agreement with what is seen on the streak camera images.

The amplitude of the limit cycle (maximum amplitude of the main body) is found to be near $\pi/2$ on the streak camera images. This value corresponds to the value of $\hat{r}_t$ at which the driving force F_{S1} is cancelled by the damping term in Eq. (14). If all of the charge were in the main body, our machine parameters would predict a larger limiting value for $\hat{r}_t$. Since the 2 mA bunch loses substantial current during its growth, the driving force is correspondingly reduced (Fig. 10).

The linear growth and the nonlinear effect leading to saturation have now been described. The relaxation of the oscillation comes from the reduction of growth due to the leakage of particles away from the main body and the formation of a new attractor close to the center of phase space.

E. Damping of system

During filamentation, an escaping particle spirals towards the center, with a resultant increase in its synchrotron frequency. As derived using the KBM method, the net force on any particle is the average over one of its synchrotron periods, $2\pi/\omega_{st}$. During each integration time, the escaping particle precesses in $\Delta\phi$, and the forces acting on it vary in amplitude. When the particle is π out of phase with the main body, for example, it is strongly damped by the wake field. As it spirals toward the center, it alternately experiences positive and negative forces from the main body wake field. Over a rotation of $\Delta\phi=2\pi$, the net growth due to this wake field nearly vanishes, so the particle damps in a time longer than the radiation damping time, 10 ms in our experiment. The escaping test particle also generates a wake field. Obviously, this wake field provides a growth term to the net force this particle experiences. Other escaping particles will enhance this growth term when they are in phase with the test particle. Consequently, the larger the charge of the escaping particle, the slower its overall damping.

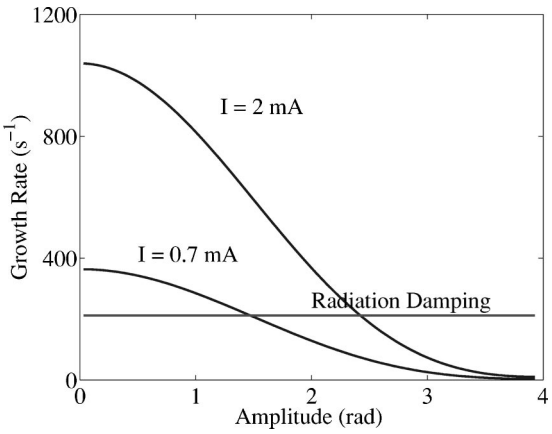

FIG. 10. Growth rate of center of mass (i.e., main body), which carries all of the charge, as a function of its radial position in the bucket. The distance at which the force acting on a 2 mA bunch would be cancelled by damping would be at 2.4 radians. However, the bunch loses its charge density during the growth as filamentation develops. A current of 0.7 mA remaining in the main body is exactly compensated by the incoherent damping when the main body reaches its limit cycle.

From Eqs. (13) and (15),

$$\lim_{r_t\to 0}\dot{\bar{\phi}}_t \propto \lim_{r_t\to 0}\frac{F_{C1}}{\bar{r}_t}\propto J_1(\bar{r}_u)\frac{1}{\bar{r}_t}\cos(\Delta\phi+\phi^*),$$

where ϕ^* is a constant. Since there always exists a coordinate pair $(\bar{r}_t,\Delta\phi)$ that can provide any desired $\dot{\bar{\phi}}_t$, there always exist points which are in phase with the main body. On the locus of such points is a fixed point at which the radial growth vanishes. If our system were static, this fixed point would be an attractor. Since our system is dynamic, the attractor location moves. It moves very slowly, so its $\dot{\bar{r}}$ is small. Therefore, the attractor lies close to the fixed point defined above. This new attractor is initially located very near the origin, where the wake-field-induced frequency shift varies rapidly.

The escaping test particle needs to reach the line where the main body exerts no radial force, which is about $\pi/2$ away from the line of maximal growth. For $\omega_z=\omega_{so}$, this line is close to $\phi=0$, i.e., close to the main body. As this attractor accumulates more charge, its self-generated wake increases in strength. To compensate for this, the attractor must see more damping from the main body and must move further away azimuthally, i.e., $\Delta\phi$ needs to increase. As it captures more particles, this attractor moves further away from the center. It becomes the new main body in the next relaxation cycle.

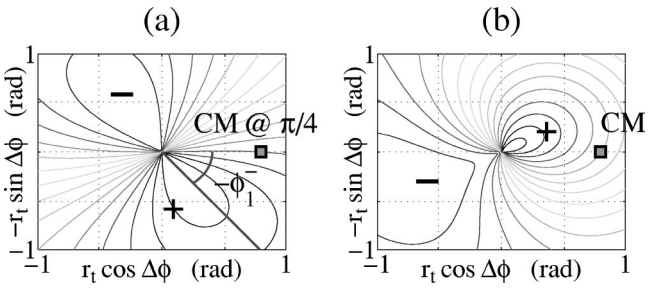

FIG. 11. Amplitude of $\bar{r}$ and $\bar{\phi}$ in rotating phase space. Same conditions as in Fig. 9, but with $\omega_z > \omega_{so}$ ($\omega_z = 1.4\omega_{so}$). (a) The quadrature component of the wake field; (b) The in-phase component of the wake field. The amplitudes of these terms are nearly identical to those of Fig. 9, but rotated by $-\phi_1^-$; in particular, the rotation of (a) justifies why the damping process takes longer than in the case of $\omega_z = \omega_{so}$.

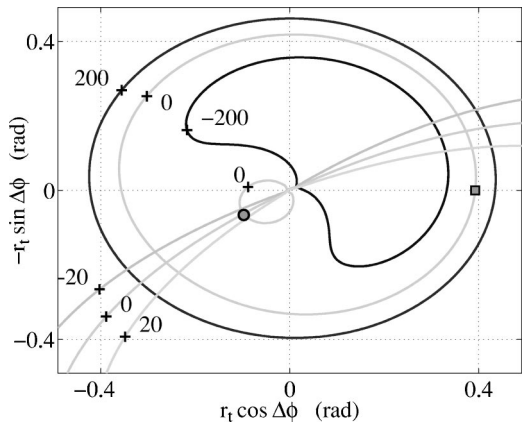

FIG. 12. Phase space contour lines of $\bar{r}_t = 0$ (contour levels of -20, 0, 20 displayed) and $\bar{\phi}_t - \bar{\phi}_u = 0 = 0$ (contour levels of -200, 0, 200 displayed). The CM at ($\bar{r}_u = \pi/8$, $\bar{\phi}_u = 0$) carries 60% of the 2 mA current; the test particle at ($\bar{r}_t, \bar{\phi}_t$) carries the rest; $\omega_z = 1.4\,\omega_{so}$. The second attractor is near the intersection of the zero level lines; particles at that location do not grow or damp and are locked in phase with the main body with a $\Delta\phi$ close to π.

F. Visualization of second attractor

A particularly interesting case appears when the lower edge of the resonance coincides with the synchrotron sideband ($\omega_z > \omega_{so}$). In this case, the second attractor forms away from the center nearly π out of phase with the main initial body and the damping time of the system is much longer than when $\omega_z = \omega_{so}$.

Defining $\phi_1^{\pm}$ such that

$$\sin\phi_1^{\pm} = \frac{(\omega_{su} \pm \omega_z)}{\sqrt{\alpha_R^2 + (\omega_{su} \pm \omega_z)^2}},$$
$$\cos\phi_1^{\pm} = \frac{\alpha_R}{\sqrt{\alpha_R^2 + (\omega_{su} \pm \omega_z)^2}}, \tag{16}$$

and, keeping only the leading terms, Eqs. (12) and (13) can be written as

$$F_{S1\approx} = -\frac{\omega_{s_0}^2}{V_{RF}|\cos\varphi_s|} 2\alpha_R R_S I J_1(r_u)[J_0(r_t) + J_2(r_t)] \times \left[\frac{\cos(\phi_1^- + \Delta\phi)}{\sqrt{\alpha_R^2 + (\omega_{su} - \omega_z)^2}} - \frac{\cos(\phi_1^+ + \Delta\phi)}{\sqrt{\alpha_R^2 + (\omega_{su} + \omega_z)^2}}\right], \tag{17}$$

$$F_{C1\approx} = \frac{\omega_{s_0}^2}{V_{RF}|\cos\varphi_s|} 2\alpha_R R_S I \left\{ 2\frac{\omega_z}{\alpha_R^2 + \omega_z^2} J_0(r_u) J_1(r_t) + J_1(r_u)[J_0(r_t) - J_2(r_t)] \left[\frac{\sin(\phi_1^- + \Delta\phi)}{\sqrt{\alpha_R^2 + (\omega_{su} - \omega_z)^2}} - \frac{\sin(\phi_1^+ + \Delta\phi)}{\sqrt{\alpha_R^2 + (\omega_{su} + \omega_z)^2}}\right]\right\}. \tag{18}$$

In our case of interest, i.e., when ω_z is larger than ω_{so}, the dominant terms of Eqs. (17) and (18) are

$$F_{S1\approx} = -\frac{\omega_{s_0}^2}{V_{RF}|\cos\varphi_s|} 2\alpha_R R_S I J_1(r_u)[J_0(r_t) + J_2(r_t)] \times \frac{\cos(\phi_1^- + \Delta\phi)}{\sqrt{\alpha_R^2 + (\omega_{su} - \omega_z)^2}},$$

$$F_{C1\approx} = \frac{\omega_{s_0}^2}{V_{RF}|\cos\varphi_s|} 2\alpha_R R_S I \left\{ 2\frac{\omega_z}{\alpha_R^2 + \omega_z^2} J_0(r_u) J_1(r_t) + J_1(r_u)[J_0(r_t) - J_2(r_t)] \frac{\sin(\phi_1^- + \Delta\phi)}{\sqrt{\alpha_R^2 + (\omega_{su} - \omega_z)^2}}\right\}.$$

The distributions of damping and growth from the $F_{S1\approx}$ function and of frequency shift from the $F_{C1\approx}$ function are, to first order, the same as those of the case where $\omega_z = \omega_{so}$, but rotated by $-\phi_1^-$ (Fig. 11). (Note that from its definition in Eq. (16), ϕ_1^- is negative when $\omega_z > \omega_{so}$.)

For $\omega_z = \omega_{so}$, the line of maximum growth is defined by $\Delta\phi = 0$. On this line, the wake-induced frequency shift is close to zero. For $\omega_z > \omega_{so}$, this line of maximum growth is now located at $\Delta\phi = -\phi_1^-$.

The behavior of a test particle near the main body is now qualitatively examined as in Sec. VI D.

(1) A test particle attempting to leave the rear of the bunch has smaller growth, so Δr, its radial position with respect to that of the main body, decreases. Both the wake field and pendulum frequency shifts move it back towards the main body, as before for $\omega_z = \omega_{so}$. This recapture is similar to the cases described in Sec. VI D for $\Delta r = 0$ and $\Delta r > 0$.

(2) A test particle at ($\Delta r < 0$, $\Delta\phi = 0$) now has a more difficult time leaving the head of the bunch for two reasons:

(i) as the particle acquires some $+\Delta\phi$, it moves closer to the line of maximal growth, located at $-\phi_1^-$, where the

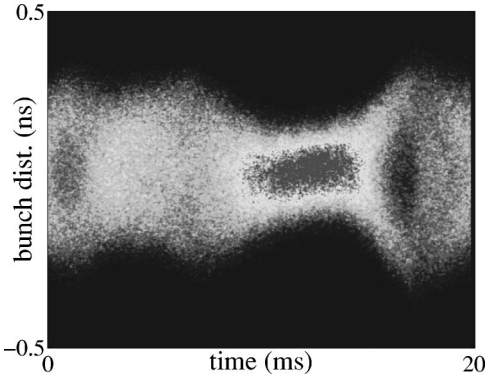

FIG. 13. Relaxation oscillation for $h=751$ ($f_{HOM}=961.6$ MHz) HOM.

wake field pushes it out radially and the pendulum slows it down; (ii) the test particle will need to precess $\Delta\phi=2|\phi_1^-|$ before its radial growth is less than that of the main body.

Accordingly, it will take much longer for the particles to escape from the bunch. Longer damping times of the relaxation oscillation for $\omega_z>\omega_{so}$ have been observed experimentally (Fig. 3).

As discussed in Sec. VI E, a second attractor, which is locked in phase with the main body, forms nearly $\pi/2$ away from the line of maximal growth. Since this line is already located at $-\phi_1^-$, the additional $\pi/2$ places the second attractor close to π out of phase with the main body (Fig. 12).

This two-particle model has described the complicated behavior observed on the streak camera in Fig. 7 and described in Sec. III C 2. The model explains the growth as a macroparticle, the filamentation and loss of charge density during this growth, the formation of a second attractor near the origin, the flow of particles from the first attractor to the second, and the eventual growth of this second attractor while the first is still visible. The second attractor is most clearly visible in the case of $\omega_z>\omega_{so}$, when the two attractors are phase locked nearly π apart.

VII. GENERALIZATION TO ANY HOM

This analysis also extends to true HOMs. The amplitude of saturation is still determined by the decrease of the driving term and the loss of charge density in the main body as the radial amplitude increases, as presented in Fig. 13. The arguments of the Bessel functions are now changed to $r_t=\hat{\tau}_t\omega_{HOM}$ and $r_u=\hat{\tau}_u\omega_{HOM}$. Since the angular HOM frequency ω_{HOM} is greater than ω_{RF}, the saturation occurs for smaller radial amplitude. Since the pendulum equation still comes from the accelerating voltage, oscillating at frequency ω_{RF}, the pendulum frequency shift at saturation, $\frac{1}{16}(\hat{\tau}_t\omega_{RF})^2\omega_{so}$, is much smaller than that observed for the case of the fundamental.

The analytical approach is also valid for multibunch cases. For example, for N equally distributed bunches, instead of decomposing ω_{RF} in $p\omega_o+\omega_z$, ω_{RF} must now be expressed as $nN\omega_o+(m\omega_o+\omega_z)$, $0\leqslant m<N$, giving the expected N modes of the system. The derivation is straightforward and is omitted here.

Experimental data was obtained on SPEAR with seven bunches in the presence of a strong HOM at 961 MHz. As shown in Figs. 1 and 13, the relaxation oscillation frequency is also smaller than 100 Hz. These data verify that this analysis holds for general HOMs. As seen in Fig. 13, the saturation amplitude scales with the ratio of ω_{RF}/ω_{HOM}.

VIII. CONCLUSION

In this paper we have analyzed the characteristics of the longitudinal relaxation oscillations, long observed in many machines, generated in the presence of narrow-band impedances. Extensive experimental measurements were performed at SPEAR. An enhanced simulation code provided helpful insights into the mechanism involved. An analytical method was presented that derives a simple model that explains the important features of the oscillation.

Although this model has been very successful in describing the essential characteristics of this relaxation oscillation, it is hoped that further refinements bring even better agreement with experimental data. The model likely needs to be extended beyond a two-particle system, possibly to a continuous distribution. This extension should better explain the radial amplitude of the second attractor in the case of large amplitudes of the main body. Work on the tracking code continues in parallel.

ACKNOWLEDGMENTS

We are very grateful to A. Hofmann, S. Heifets, and A. Chao for valuable discussions. We also thank H. Wiedemann and M. Cornacchia for their support and encouragement. Finally, we would like to thank our colleagues J. Hinkson and J. Byrd (LBNL), A. Fisher (SLAC), and A. Lumpkin (APS) for their assistance in obtaining the beautiful pictures with the streak camera.

APPENDIX: NUMERICAL COMPUTATION OF WAKE IN SIMULATION PROGRAM

In the multiparticle tracking code, the wake field must be computed on short time scales, i.e., many time divisions per rms bunch length, and must be carried over long time scales to the next bunch.

The longitudinal wake for a resonator of resistance R_s, frequency $\bar{\omega}$, of damping rate α_R and quality factor Q is

$$W(t-\tau)=U(t-\tau)2\alpha_R R_s e^{-\alpha_R(t-\tau)}\left\{\cos[\bar{\omega}(t-\tau)]-\frac{\alpha_R}{\bar{\omega}}\sin[\bar{\omega}(t-\tau)]\right\}$$

with

$$\alpha_R=\frac{\omega_R}{2Q}\ \text{ and }\ \bar{\omega}=\sqrt{\omega_R^2-\alpha_R^2},$$

where $U(t)$ is the Heaviside function:

$$U(t)=\begin{cases} 1 & t>0 \\ 1/2 & t=0 \\ 0 & t>0 \end{cases}.$$

In the simulation, for the purpose of the calculation of the wake, particles are grouped into discrete bins of width Δt. The wake is then represented as a set of discrete steps, one step per bin. The wake in a given bin $t+\Delta t$ is the sum of the wake from the previous bin t transported over one bin and the contribution from the particles in the current bin. From the fundamental theorem of beam loading, a particle sees only one half of its instantaneous wake, whereas all subsequent particles see all of this wake. Since the fields obey the second order wave equations, the propagator can be described by

$$\begin{pmatrix} W(t+\Delta t) \\ W'(t+\Delta t) \end{pmatrix} = e^{-\alpha \Delta t} \begin{pmatrix} \cos(\omega_R' \Delta t) & \frac{1}{\omega_R'} \sin(\omega_R' \Delta t) \\ -\omega_R' \sin(\omega_R' \Delta t) & \cos(\omega_R' \Delta t) \end{pmatrix} \times \begin{pmatrix} W(t)+\alpha R_s n(t) \\ W'(t)-2\alpha^2 R_s n(t) \end{pmatrix} + \begin{pmatrix} \alpha R_s n(t+\Delta t) \\ -2\alpha^2 R_s n(t+\Delta t) \end{pmatrix}.$$

Since the bin spacing is fixed, this bin-to-bin propagator is a constant matrix that can be calculated once, and then be used repeatedly. The derivative of the wake must also be computed and carried along.

[1] E. D. Courant and H. S. Snyder, Ann. Phys. (N.Y.) **3**, 1 (1958).

[2] H. Huang *et al.*, Phys. Rev. E **48**, 4678 (1993).

[3] J. M. Byrd, W. H. Cheng, and F. Zimmermann, Phys. Rev. E **57**, 4706 (1998).

[4] Y. Yamazaki, H. Kobayakawa, Y. Kamiya, and M. Kihara (unpublished).

[5] G. Rakowsky, in *Proceedings of the Particle Accelerator Conference 85* (IEEE-APS, Vancouver, 1985), pp. 2377–2379.

[6] A. Wrulich *et al.*, in *Proceedings of the European Particle Accelerator Conference 96* (CERN, Sitges, 1996), pp. 1108–1110.

[7] A. W. Chao, *Physics of Collective Beam Instabilities in High Energy Accelerators* (John Wiley, New York, 1993).

[8] C. Limborg and J. Sebek, in *Proceedings of the European Particle Accelerator Conference 98* (CERN, Stockholm, 1998), pp. 972–974.

[9] J. Sebek and C. Limborg, in *Proceedings of the 1997 International Committee for Future Accelerators Conference, Frascati Physics Series*, edited by L. Palumbo (LNF/INFN, Frascati, 1997).

[10] K. W. Robinson (unpublished).

[11] *Using MATLAB* (The MathWorks, Inc., Natick, MA, 1996).

[12] T. Suzuki and K. Yokoya, Nucl. Instrum. Methods Phys. Res. **203**, 45 (1982).

[13] R. Nagaoka and A. Wrulich, in *Proceedings of EPAC96* (CERN, Sitges, 1996), pp. 316–318.

[14] N. M. Krylov and N. N. Bogoliubov, *Introduction to Nonlinear Mechanics. Annals of Mathematical Studies* (Princeton University Press, Princeton, 1947).

[15] N. N. Bogoliubov and Y. A. Mitropolsky, *Asymptotic Methods in the Theory of Nonlinear Oscillations* (Gordon and Breach Science Publishers, New York, 1961).

[16] E. A. Jackson, *Perspectives of Nonlinear Dynamics* (Cambridge University Press, Cambridge, 1989), Vol. 1.

[17] S. Krinsky, in *Proceedings of PAC85* (IEEE-APS, Vancouver, 1985), pp. 2320–2322.

[18] A. Hofmann, in *Proceedings of CAS 1993*, Vol. 1 of *CAS*, edited by S. Turner (CERN, Geneva, 1995), pp. 307–330.